Journal of Magnetic Resonance **157,** 253–266 (2002)
doi:10.1006/jmre.2002.2594

Double-Quantum Dipolar Recoupling at High Magic-Angle Spinning Rates

Per Eugen Kristiansen,* Dan J. Mitchell,† and Jeremy N. S. Evans*,†,[1]

*School of Molecular Biosciences, and †Center for NMR Spectroscopy, Washington State University, Pullman, Washington 99164-4660

Received February 5, 2002; revised June 13, 2002

A full investigation of the possible homonuclear double-quantum recoupling sequences, based on the *RN* family of sequences with $N \leq 20$, is given. Several new *RN* sequences, $R16^5_6$, $R18^5_8$, and $R18^5_{10}$, were applied at high magic-angle spinning rates and compared with theory. The $R18^5_{10}$ technique can be used to recouple dipolar couplings at spinning rates up to 39 kHz, and the application of the sequence in an INADEQUATE experiment is shown for a spinning rate of 30 kHz. © 2002 Elsevier Science (USA)

Key Words: **solid-state NMR; high-frequency MAS; simulations; DQ recoupling; assignment methods.**

1. INTRODUCTION

Solid-state nuclear magnetic resonance (NMR)[2] is useful for determining biomolecular structures from measurement of internuclear distances (*1–16*) and dihedral angles (*17–20*). Application of solid-state NMR to biomolecular systems such as enzymes (*21–24*), membrane proteins (*25, 26*), and amylogenic proteins (*27, 28*) has yielded information that is difficult or unobtainable by other structural methods, such as liquid-state NMR and X-ray crystallography. However, one of the limitations in the application of solid-state NMR to biomolecules is the lack of resolution and sensitivity (*29, 30*), although with the advent of high-field magnets, increased resolution has been achieved (*31*).

It has been shown empirically that the resolution is strongly dependent on the magic-angle spinning (MAS) speed and proton decoupling power (*32, 33*). The chemical-shift anisotropy (CSA) is magnetic field dependent, and requires an increasing spinning rate with increasing field. This removes rotational side bands from the spectrum and increases resolution, as well as helping to remove anisotropic dependencies. While solid-state MAS NMR has the potential to provide the necessary spectral resolution for biomolecular systems, it tends to average interactions that contain important structural information. Therefore it is necessary to reintroduce these interactions in order to obtain information about their magnitude and direction. Several dipolar recoupling techniques have been developed during the last decade (reviewed in *34*). Currently, few techniques are able to recouple the homonuclear dipolar couplings between low gamma nuclei effectively, while at the same time decoupling the protons. Many of these recoupling techniques depend on the rf power on the recoupled S-spin (^{13}C in our case) channel (ω^S_{nut}), being matched to the rotor spinning frequency (ω_R) (*9, 13–15, 35*). For instance with the C7 sequence, the rf power on the S channel needs to be 7 times the rotor speed ($\omega^S_{nut} = 7\omega_R$) (*13*). At the same time as these recoupling techniques are applied to the S spins, the rf-decoupling power of the I spins (^{1}H in our case) need to be adjusted to give maximum signal. It has been shown empirically that the rf power of the proton decoupling for most of these sequences needs to be approximately $\omega^I_{nut} = 3\omega^S_{nut}$ (*35–37*). However, most commercial solid-state NMR probes that are used in solid-state NMR have restricted power capabilities, which often severely limits the use of several of these sequences at high MAS rates. During the past couple of years, new dipolar recoupling techniques with lower power requirements have been designed. Hohwy *et al.* (*35*) introduced the SPC5 (supercycled post C5), that only requires $\omega^S_{nut} = 5\omega_R$. Brinkmann *et al.* (*37*) have since introduced a supercycled $C14^5_4$ (SPC14) that only requires $\omega^S_{nut} = 3.5\omega_R$. In practice, however, even with these sequences, one is limited to spinning rates below 20 kHz. The RFDR-type of zero quantum recoupling techniques are, however, the only sequences known to us that so far have been able to recouple low gamma nuclei at spinning rates of more than 20 kHz (*31, 38*). Development of new, efficient DQ dipolar recoupling techniques that can be used at spinning rates above 20 kHz are therefore needed.

Several of the recoupling techniques noted above have been successfully applied to multidimensional NMR assignments. Double-quantum recoupling techniques can, for instance, be used in experiments similar to the solution-state INADEQUATE experiment. The INADEQUATE experiment has, in solids, been shown to give better resolution in the second dimension compared to other types of recoupling experiments, and this was claimed to be partly due to the double-quantum evolution in the t_1 dimension being "double" in double-quantum spectroscopy (*39*).

[1] To whom correspondence should be addressed. E-mail: evansj@wsu.edu.

[2] *Abbreviations used*: CSA, chemical-shift anisotropy; DQ, double quantum; ICS, isotropic chemical shift; MAS, magic-angle spinning; NMR, nuclear magnetic resonance; TPPI, time-proportional phase incrementation; TPPM, two-pulse phase modulation.

1090-7807/02 $35.00
© 2002 Elsevier Science (USA)
All rights reserved.

While indirect detection of low gamma nuclei via protons is standard in liquid-state NMR of biomolecules, most techniques used in solid-state NMR of biomolecules are based on direct detection. It has, however, been shown that the sensitivity enhancement by indirect detection on ^{1}H is possible in solid-state NMR (*40, 41*). For the signal enhancement to be realized, spinning rates high enough to efficiently remove the dipolar couplings between protons are needed (*40, 41*). Furthermore, techniques that efficiently recouple the dipolar couplings between high gamma nuclei for distance determination, or between low gamma nuclei as a part of a resolution-enhancement approach, are needed. For distance measurements between protons, sequences that can be used for recoupling at frequencies of 30 and 50 kHz are needed, which in practice means sequences with the relationship $\omega^S_{nut}/\omega_R \approx 3$ between spinning speed and rf power. So far, the only efficient DQ dipolar recoupling sequences that are known with this property are the SPC14 (*37*) and the $R14^5_4$ (*16, 42*), and the development of new sequences is therefore needed.

Recently, a set of rules for designing symmetric pulse sequences, called the RN^ν_n symmetries, was published (*16*). Here we are investigating pulse sequences that selectively recouple the double-quantum dipolar coupling tensor $T^D_{2\pm2}$ with the MAS rate $5 > \omega^S_{nut}/\omega_R > 1$.

2. BACKGROUND/THEORY

The RN^ν_n pulse sequence is shown in Fig. 1A. The RN^ν_n sequences consist of the basic elements R and R', which are π pulses or composite pulses giving an overall spin rotation of p radians (*16*). In cases where R consists of multiple of π phase-changed elements, R and R' are equal, and in all other cases the two elements are different (*43*). N, n, and υ are integers that are called the symmetry number of the pulse sequence. N is the number of R elements in a sequence, n is the total number of rotor cycles, and υ determines the rf phase change such that $\varphi = 180\ \upsilon/N$. Carravetta *et al.* (*16*) give the following R elements in their paper: 180, 90_0270_{180}, and $60_0300_{180}60_0$, although in principle, any broadbanded pulse giving a p phase change can be used. The off-resonance properties of a properly constructed composite pulse can generally be improved over the simple 180° rf pulses, and these pulses should have beneficial properties in broadbanded DQ dipolar recoupling.

The RN^ν_n pulse sequences recouple the first-order average Hamilton ($\bar{H}_{lm\lambda\mu}$) according to the following selection rule (*16*),

$$\bar{H}^\Lambda_{lm\lambda\mu} = 0 \quad \text{if } mn - \mu\upsilon \neq NZ_\lambda/2, \qquad [1]$$

where Z_l can be any given odd integer if λ is odd, and an even integer if λ is even. The quantum numbers l and λ are the rank of the spatial tensor A^Λ_{lm} and the spin tensor $T^\Lambda_{\lambda\mu}$ for any interaction Λ, respectively, where l and λ take values between 0 and 2 (*44*), m can take the values $-l, (-l+1), \ldots (l-1), +l$, and μ the values $-\lambda, (-l+1), \ldots (l+1), +\lambda$. From this selection rule, it can easily be seen that all possible RN sequences will recouple the J-coupling Hamiltonian ($\bar{H}_{0000}$). Other average Hamiltonians can be selected by designing a sequence that recouples the selected tensors.

The selection rule for the second-order average Hamiltonian has been shown to be (*16*)

$$\bar{H}^{(2)}_{l_2m_2\lambda_2\mu_2;l_1m_1\lambda_1\mu_1} = 0, \qquad [2]$$

$$\text{if} \begin{cases} m_1 n - \mu_1 \upsilon \neq \frac{NZ_{\lambda 1}}{2} & [2a] \\ m_2 n - \mu_2 \upsilon \neq \frac{NZ_{\lambda 2}}{2} & [2b] \\ (m_1+m_2)n - (\mu_1+\mu_2)\upsilon \neq \frac{NZ_{\lambda 1+\lambda 2}}{2} & [2c] \end{cases}$$

The symmetry-allowed terms in the first-order average Hamiltonian of the Magnus expansion has the following form (*43*),

$$\bar{H}^\Lambda_{lm\lambda\mu} = \kappa_{lm\lambda\mu}\left[A^\Lambda_{lm}\right]^R \exp\left\{-im\left(\alpha^0_{RL} - \omega_r t^0_0\right)\right\} T^\Lambda_{\lambda\mu} \qquad [3]$$

where $\kappa_{lm\lambda\mu}$ is a scaling factor for the symmetry-allowed term with quantum numbers l, m, λ, and μ; α^0_{RL} is the rotor position at time t^0_0; and t^0_0 is the time point at the start of the first R element as shown in Fig. 1.

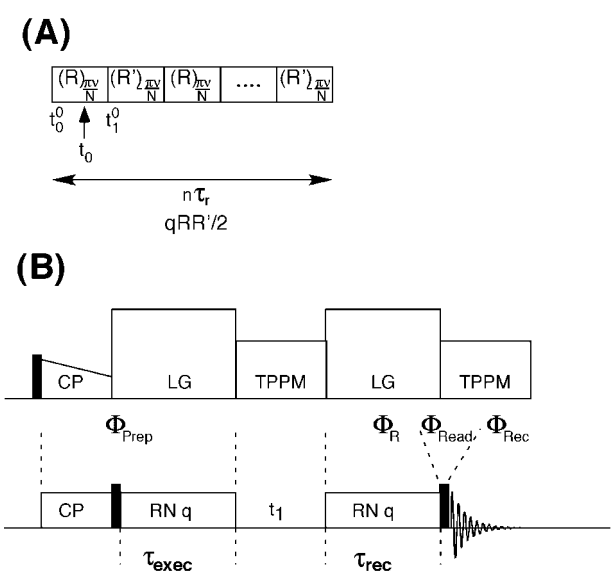

FIG. 1. The basic *RN* sequence is shown in (A) with the same timing and naming used on the sequences as in the equations. (B) The sequence used to obtain DQ recoupling in which the t_1 was kept equal to zero in distance measurements, and incremented in the INADEQUATE type of experiments.

Scaling Factor

Brinkmann and Levitt (*43*) have shown that the scaling factor $\kappa_{lm\lambda\mu}$ can be described as a function of pulse sequence elements

R in the following way,

$$\kappa_{lm\lambda\mu} = d^{l}_{m0}(\beta_{RL}) \exp\left\{-\frac{i\mu\pi\nu}{N}\right\} K_{m\lambda\mu}, \qquad [4]$$

where $d^{l}_{m,0}(\beta)$ is the reduced Wigner rotation matrix elements, and β_{RL} is the Euler angle between the mechanical rotation axis and the external magnetic field. The factor $K_{m\lambda\mu}$ has been shown to be (*43*)

$$K_{m\lambda\mu} = \tau_E^{-1} \int_0^{\tau_E} dt^0 \, d^{\lambda}_{\mu 0}(-\beta^0) \exp\{i(\mu\gamma^0 + m\omega_r t^0)\}, \qquad [5]$$

where τ_E is the duration of any R element ($t_0^1 - t_0^0$ in Fig. 1a), t^0 is a time point in the basic element, where $0 < t^0 < \tau_E$; and β^0 and γ^0 are the rotation angles at time point t^0. In this paper, we use elements that only are amplitude-modulated rf fields (all phase changes are a multiple of π), so β^0 and γ^0 are defined in terms of the basic element as (*43*)

$$\beta^0 = \int_0^{t^0} dt \omega^S_{nut}(t) \qquad [6]$$

$$\gamma^0 = \frac{\pi}{2} \qquad [7]$$

where $\omega^S_{nut}(t)$ is stepped so that it gives ω^S_{nut} positive values for the 0° phase pulses and negative values for the π phase pulses.

3. RESULTS AND DISCUSSION

Analysis of the Selection Rule

Before showing all the DQ dipolar recoupling sequences, there are some relations that can be obtained from the selection rule for the first-order average Hamiltonian given in Eq. [1] that can help in the search for *RN* sequences. Furthermore, in this subsection we will investigate other properties that can be drawn from the first- and second-order average Hamiltonian selection rules (Eqs. [1] and [2]).

There are only four pairs of quantum numbers that recouple DQ homonuclear dipolar couplings, and these are $lm\lambda\mu$, equal to 212–2 and 2–122, 2122 and 2–12–2, 222–2 and 2–222, and 2222 and 2–22–2. When the sample is spinning at the magic-angle, the terms with the quantum numbers 202 ± 2 are averaged out (*44*). For homonuclear DQ recoupling sequences, Z will always have to be even, since λ is equal to 2, and Eq. [1] can be simplified to

$$\bar{H}^{\Lambda}_{lm\lambda\mu} = 0 \quad \text{if } mn - \mu\nu \neq NZ', \qquad [8]$$

where Z' can be any integer such that NZ' is always an even integer. From this, it is obvious that sequences that recouple the average Hamiltonian $\bar{H}_{2\pm22\pm2}$ also recouple the single-quantum term $\bar{H}_{2\pm12\pm1}$, and these sequences are therefore not expected to be efficient when used in DQ recoupling, so they were excluded from further investigation.

It can be seen from the above selection rule (Eq. [8]) that for every RN^{ν}_{n} sequence there is an $RN^{N-\nu}_{n}$ sequence that recouples the average Hamiltonian with a μ quantum number of the opposite sign (Eqs. [9] and [10]),

$$mn - \mu(N - \nu) \neq NZ' \qquad [9]$$

$$mn + \mu\nu \neq NZ' + \mu N, \qquad [10]$$

where $N\mu$ is always an even number, and N has to be even. A change in the symmetry number ν to N–n is therefore the same as changing the sign of the symmetry number, and the recoupled quantum number from μ to $-\mu$. One needs therefore only to look for sequences that recouple one of the average DQ Hamiltonians, for instance $\bar{H}_{212-2}$, to find all symmetries by searching through $1 \leq n < N$.

Eighty-eight RN^{ν}_{n} sequences were found among $6 \leq N \leq 20$, $1 \leq n < N$, and $0 \leq n < N$ that only recouple the first-order average DQ Hamiltonians $\bar{H}_{2\pm12\pm2}$. The sequences that recouple the $\bar{H}_{2-122}$ and $\bar{H}_{212-2}$ Hamiltonians are shown in Table 1, together with their ω^S_{nut}/ω_R values, a factor that determines which spinning rates the sequences are suited for. All the sequences in Table 1 have $-N/2 \leq n \leq N/2$, as carried out by Carravetta *et al.* in Ref. (*16*), by making use of Eq. [10]. As shown above, sequences that recouple the $\bar{H}_{2122}$ and $\bar{H}_{2-12-2}$ Hamiltonians can be found by changing the sign of the n symmetry number of the sequences given in Table 1.

One of the DQ recoupling sequences in Table 1 is $R16^5_6$. In Fig. 2, the selection pathway of this sequence is described by a space-spin selection diagram similar to the one introduced by Feng *et al.* (*17*). It is clear that the $R16^5_6$ sequence recouples the DQ dipolar average Hamiltonian shown in Fig. 2A, while it suppresses the CSA term shown in Fig. 2B. A space-spin selection diagram can of course be made for all of the RN^{ν}_{n} sequences given in Table 1.

The rules that govern the number of second-order average Hamiltonians is given in Eq. [2], and from this, the number of second-order average Hamiltonian terms can be found. Equations [2] and [2a] are identical to Eq. [1]. From this, we see that all sequences having first-order average Hamiltonian terms for a given interaction Λ will also have second-order terms between this interaction and any other interaction that does not commute (Eq. [2]). While the DQ recoupling sequences given in Table 1 only recouple the dipolar DQ and J-coupling terms, the number of second-order average Hamiltonian terms, $\bar{H}^{(2)}_{l_2m_2\lambda_2\mu_2;l_1m_1\lambda_1\mu_1}$, varies between the sequences. The number of second-order cross terms does not depend on the sign of μ and will therefore be independent of the sign of ν.

Most of the dipolar recoupling sequences depend on the CSA to some extent. One measure of the *RN* sequences dependence of the CSA is the number of second-order cross terms between the dipolar coupling and the CSA. The $R14^6_2$ sequence has, for

TABLE 1
All of the DQ Dipolar RN_n^ν Recoupling Sequences with $N \leq 20$, $n \leq N$

	Second-order Hamiltonians between the dipolar coupling:			κ_{212-2} for the following R elements			ω_{nut}^S/ω_r			
RN_n^ν	Dipolar	CSA	ICS	180	90–270	60–300–60	180	90–270	60–300–60	$\lvert\frac{180\nu}{N}\rvert$
$R12_2^{-1}$	24	36	8	0.174	0.170	0.131	3	6	7	15°
$R12_2^5$	24	36	8	0.174	0.170	0.131	3	6	7	75°
$R12_{10}^1$	24	36	8	0.110	0.041	0.053	0.6	1.2	1.4	15°
$R12_{10}^{?5}$	24	36	8	0.110	0.041	0.053	0.6	1.2	1.4	75°
$R14_2^{-1}$	24	34	4	0.174	0.172	0.132	3.5	7	8.17	12.9°
$R14_2^6$	48	16	4	0.174	0.172	0.132	3.5	7	8.17	77.1°
$R14_4^{-2}$	48	16	4	0.168	0.157	0.122	1.75	3.5	4.08	25.7°
$R14_4^5$	24	34	4	0.168	0.157	0.122	1.75	3.5	4.08	64.3°
$R14_6^{-3}$	24	34	4	0.157	0.134	0.108	1.17	2.33	2.72	38.6°
$R14_6^4$	48	16	4	0.157	0.134	0.108	1.17	2.33	2.72	51.4°
$R14_8^3$	24	34	4	0.143	0.105	0.089	0.88	1.75	2.04	38.6°
$R14_8^{-4}$	48	16	4	0.143	0.105	0.089	0.88	1.75	2.04	51.4°
$R14_{10}^2$	48	16	4	0.126	0.071	0.069	0.7	1.4	1.63	25.7°
$R14_{10}^{-5}$	24	34	4	0.126	0.071	0.069	0.7	1.4	1.63	64.3°
$R14_{12}^1$	24	34	4	0.107	0.035	0.062	0.58	1.17	1.36	12.9°
$R14_{12}^{-6}$	48	16	4	0.107	0.035	0.062	0.58	1.17	1.36	77.1°
$R16_2^{-1}$	24	30	4	0.175	0.173	0.133	4	8	9.33	11.3°
$R16_2^7$	24	30	4	0.175	0.173	0.133	4	8	9.33	78.7°
$R16_6^{-3}$	24	30	4	0.161	0.143	0.114	1.33	2.67	3.11	33.8°
$R16_6^5$	24	30	4	0.161	0.143	0.114	1.33	2.67	3.11	56.3°
$R16_{10}^3$	24	30	4	0.136	0.092	0.082	0.8	1.6	1.87	33.8°
$R16_{10}^{-5}$	24	30	4	0.136	0.092	0.082	0.8	1.6	1.87	56.3°
$R16_{14}^1$	24	30	4	0.105	0.030	0.047	0.57	1.14	1.33	11.3°
$R16_{14}^{-7}$	24	30	4	0.105	0.030	0.047	0.57	1.14	1.33	78.7°
$R18_2^{-1}$	24	22	4	0.175	0.174	0.133	4.5	9	10.5	10°
$R18_2^8$	32	16	4	0.175	0.174	0.133	4.5	9	10.5	80°
$R18_4^{-2}$	32	16	4	0.171	0.165	0.127	2.25	4.5	5.25	20°
$R18_4^7$	24	22	4	0.171	0.165	0.127	2.25	4.5	5.25	70°
$R18_8^{-4}$	32	16	4	0.155	0.131	0.106	1.13	2.25	2.63	40°
$R18_8^5$	24	22	4	0.155	0.131	0.106	1.13	2.25	2.63	50°
$R18_{10}^4$	32	16	4	0.144	0.108	0.092	0.9	1.8	2.1	40°
$R18_{10}^{-5}$	24	22	4	0.144	0.108	0.092	0.9	1.8	2.1	50°
$R18_{14}^2$	32	16	4	0.118	0.055	0.060	0.64	1.29	1.5	20°
$R18_{14}^{-7}$	24	22	4	0.118	0.055	0.060	0.64	1.29	1.5	70°
$R18_{16}^1$	32	22	4	0.103	0.027	0.045	0.56	1.13	1.31	10°
$R18_{16}^{-8}$	32	16	4	0.103	0.027	0.045	0.56	1.13	1.31	80°
$R20_2^{-1}$	24	20	4	0.176	0.174	0.133	5	10	11.7	9°
$R20_2^9$	24	20	4	0.176	0.174	0.133	5	10	11.7	81°
$R20_6^{-3}$	24	20	4	0.167	0.155	0.121	1.67	3.33	3.89	27°
$R20_6^7$	24	20	4	0.167	0.155	0.121	1.67	3.33	3.89	63°
$R20_{14}^3$	24	20	4	0.128	0.074	0.071	0.71	1.43	1.67	27°
$R20_{14}^{-7}$	24	20	4	0.128	0.074	0.071	0.71	1.43	1.67	63°
$R20_{18}^1$	24	20	4	0.102	0.024	0.044	0.56	1.11	1.3	9°
$R20_{18}^{-9}$	24	20	4	0.102	0.024	0.044	0.56	1.11	1.3	81°

Note. Dipolar couplings have the following recoupled Hamiltonians: $\bar{H}_{2-122}$ and $\bar{H}_{212-2}$. In columns 2–4, the numbers of second-order Hamiltonian cross terms between the dipolar coupling and other interactions are given. Three different R elements have been used in the calculated κ_{212-2} given in columns 5–7. The relationship between the spinning rate for the different sequences is given in columns 8–10, and the absolute ϕ angle value of the R element is shown in column 11.

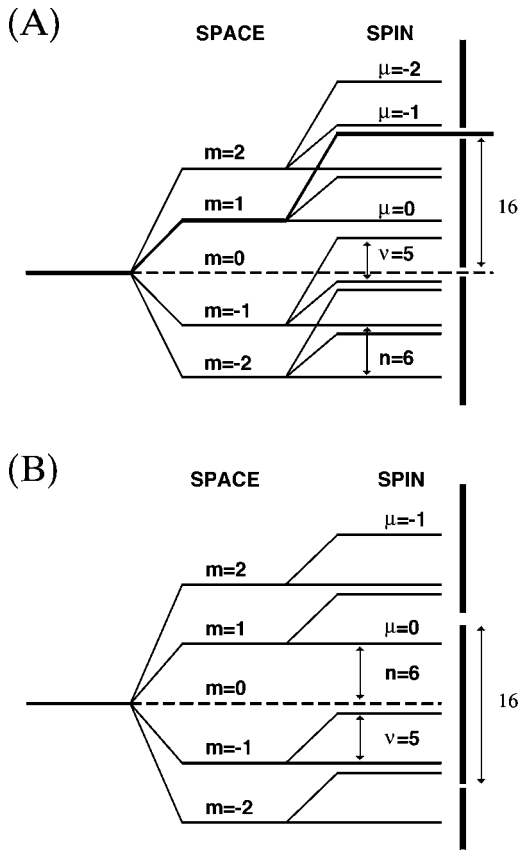

FIG. 2. The selection of (A) dipolar recoupling Hamiltonian and (B) suppression of the chemical-shift anisotropy Hamiltonian for $R16_6^5$.

instance, only 16 second-order average Hamiltonian cross terms between dipolar coupling and the CSA, and has been shown to have a very low dependence on CSA (*46*). Among the sequences expected to be of use at spinning rates between 15 and 40 kHz, the following were found to have few second-order average Hamiltonian terms between the dipolar coupling and the CSA: $R20_6^7$, and $R20_{14}^7$ have only 20 terms; and $R18_4^7$, $R18_8^5$, and $R18_{10}^5$ have 22 terms. Since all of them have less second-order cross terms between the dipolar coupling and the CSA than the $R14_4^5$ sequence (*42*) with its 34 terms, and the C7 sequence with its 54 terms (*16*), we will assume that all the sequences show relatively small CSA dependence. Other second-order cross terms might also influence the recoupling, for example, $R12_n^\nu$ sequences have 8 cross terms between the dipolar coupling and the ICS, while all other sequences found had only 4 terms, and for this reason, these sequences were assumed to be more dependent on chemical shift than all the other sequences. The number of second-order average Hamiltonian recoupling terms between the rf field and dipolar coupling was 4 for all the sequences, and 8 terms were found for the interaction between the J-coupling and the dipolar coupling. Based on the number of second-order terms alone, most sequences should be usable for DQ recoupling.

Scaling Factors

The time needed to obtain maximum double-quantum efficiency depends on the scaling factor, $\kappa_{lm\lambda\mu}$ and of course the dipolar coupling. A sequence with a small scaling factor will need longer recoupling times to reach maximal DQ efficiency, and therefore result in higher stress on the probe as compared to sequences that have larger scaling factors. Furthermore, sequences that have large scaling factors are expected to be less influenced by effects of relaxation, and therefore work better with small dipolar couplings than sequences with small scaling factors. Sequences with high scaling factors will therefore be preferable to ones with small scaling factors.

The scaling factor for all the sequences have been calculated by solving Eq. [4], the results are shown in Table 1 for the three different R elements. The absolute values of the scaling factors do not depend on ν or μ, as can be seen from Eq. [4]. For sequences with a small n, it was observed that the scaling factor decreases when the length of the R element is increased. It can also be seen from Table 1 that the scaling factor decreases with decreasing N/n. When pursuing some of the fast spinning sequences ($\omega_{nut}^S/\omega_R < 1.5$) like $R12_{10}^1$, $R12_{10}^{-5}$, $R14_{12}^{-6}$, $R16_{14}^{-7}$, $R18_{16}^{-8}$, and $R20_{18}^{-9}$, the scaling factors show that the most time-efficient recoupling (larger scaling factor) is obtained by using the R element $60_0300_{180}60_0$. These sequences should therefore need the shortest DQ recoupling time to reach a maximum in DQ efficiency with this R element. The medium-to-rapid spinning ($4 > \omega_{nut}^S/\omega_R > 1.5$) recoupling sequences such as $R16_6^5$, $R16_{10}^5$, $R18_4^7$,$R18_8^5$, $R18_{10}^{-5}$, $R18_{14}^{-7}$, $R20_6^7$, and $R20_{14}^{-7}$ have larger scaling factors with the elements 180 and 90_0270_{180} rather than with $60_0300_{180}60_0$.

Simulations

Simulated data of [2,3-$^{13}C_2$]succinic acid, [2,3-$^{13}C_2$]alanine, and [1,2-$^{13}C_2$]glycine spin systems were used to examine the properties of the various *RN* dipolar recoupling techniques. The DQ recoupling of the two-spin system of succinic acid has been simulated for all the sequences given in Table 1, and a selection of the DQ recoupling results is listed in Table 2. Empirical parameters included are the ICS and the CSA obtained from Ref. (*50*), and typical CSA tensor orientations were used. The maximum DQ recoupling efficiencies were determined from the recoupling curves obtained in numerical simulations, and are given in Table 2, together with the recoupling times. The DQ recoupling efficiency was measured as in Lee *et al.* (*13*). All of the sequences gave a DQ excitation profile approximately equal to the one observed for C7 (*13*) and $R14_2^6$(*16*), as expected from the average Hamiltonian (from $\langle \sin^2(|\omega_{jk}|\tau_{exec})\rangle$ where $\langle \ldots \rangle$ denotes the powder average) (*46*).

The succinic acid spin system was simulated to determine the susceptibility of different sequences to rf errors. Data from these simulation on the following sequences, $R14_2^6$, $R14_4^5$, $R14_4^{-2}$, $R12_{10}^5$, and $R12_{10}^{-1}$, are shown in Fig. 3. As can be seen from Fig. 3, all of these sequences are well-behaved when the R

TABLE 2
The Results from Our Simulations of DQ Recoupling Efficiency on the [2,3-$^{13}C_2$]Succinic Acid Spin System

	Overall shape of the DQ recoupled curve		DQ recoupling times[c]		DQ efficiency for the given R element in %[d]	
RN_n^v	Time evolution[a]	Rf stability[b]	90–270	60–300–60	90–270	60–300–60
$R12_2^1$	+++	−	556 μs		72.1	
$R12_2^5$	+++	+++	556 μs		72.5	
$R12_2^7$	+++	+++	556 μs		72.3	
$R12_{10}^1$	+, +	−, −	1751 μs	1682 μs	65.9	71.4
$R12_{10}^5$	−, ++	+, ++	1751 μs	1682 μs	47.0	65.5
$R14_2^6$	+++	+++	559 μs		72.8	
$R14_4^2$	++		592 μs		69.9	
$R14_4^5$	++/+++	++	592 μs		71.8	
$R14_6^4$	++		719 μs		68.8	
$R14_{10}^5$	++/+		1271 μs	1307 μs	66.6	70.9
$R14_{12}^6$	+/−, −	++, +++	1964 μs	1644 μs	38.9	62.4
$R16_2^7$	+++		528 μs		71.9	
$R16_6^5$	++	++	641 μs		69.5	
$R16_{10}^5$	++/+, +	+/++, +/−	960 μs	1124 μs	66.4	68.4
$R16_{14}^7$	−, −		1920 μs	1866 μs	30.7	59.6
$R18_2^8$	+++	+++	537 μs		72.2	
$R18_4^7$	+++	+++	584 μs		72.0	
$R18_8^5$	++, ++	++, ++	730 μs	1209 μs	72.5	71.3
$R18_{10}^5$	++	++	916 μs		71.9	
$R18_{14}^7$	+/++	++	1621 μs	1499 μs	61.9	70.6
$R18_{16}^1$	+, +	−, −	3362 μs	2101 μs	68.2	72.2
$R18_{16}^8$	−, +/−	−, −	1861 μs	1697 μs	23.1	55.6
$R20_2^9$	+++	+++	549 μs		71.9	
$R20_6^7$	++/+++	++/+++	615 μs		71.2	
$R20_{14}^7$	++, ++	++, ++	1202 μs	1309 μs	68.4	70.2
$R20_{18}^9$	−, −	+	2000 μs	1870 μs	17.4	51.9

Note. The dipolar coupling of 2150 Hz and CSA and shift values were taken from Ref. (*51*), and standard tensor orientations were used in the simulations.

[a] The following qualitative terms are used to describe the shape of the DQ recoupling curves: +++, if the curve is smooth with rapid DQ build-up and high DQ efficiency. ++, if it has a smooth DQ build-up curve. +, DQ recoupling curve is relatively smooth, with some oscillations allowed (see text for details). −, curve gives both positive and negative DQ efficiencies and/or show low DQ efficiency and have large oscillations.

[b] The following qualitative terms are used to describe the stability of the shape of DQ buildup curve toward deviations in rf power (error in ω_{nut}^S); the evaluation refers to the point with maximum DQ efficiency. +++, if the DQ efficiency curve does not change the DQ efficiency at maximum with more than 20% with rf errors of ±10%. ++, the DQ recoupling curve is positive at approximately 10% change in ω_{nut}^S. +, the DQ recoupling curve is giving positive at approximately 5% change in ω_{nut}^S. −, refers to a DQ efficiency curve that can not accept an error of 2% in ω_{nut}^S.

[c] The DQ recoupling times are the time needed to reach a maximum DQ efficiency as measured from the simulated DQ recoupling curves. In cases of bad DQ recoupling, the times refers to the first local maximum and global minimum.

[d] The DQ efficiency is given as a percentage of the signal without DQ recoupling as measured from our simulations at the global first maximum. In cases of unfavorable DQ recoupling, the efficiencies are given for the first local maximum and global minimum.

element gives exact p rotations (rf error = 0%). Inspection of the sequences shows that $R14_2^6$ (Fig. 3A) has the shortest DQ build-up time, followed by $R14_4^5$ (Fig. 3B), and $R14_4^{-2}$ (Fig. 3C). The $R12_{10}^5$ sequence given in Figs. 3D and (E), and $R12_{10}^{-1}$ (Fig. 3F) have much slower DQ build-up times, as is expected from the scaling constants. A somewhat more rapid build-up is observed for the $R12_{10}^5$ sequence, when the R element $60_0300_{180}60_0$ is applied rather than 90_0270_{180}, although the differences in DQ build-up times are less than expected from the first-order Hamiltonian scaling constant. One reason for this might be differences in the recoupling scaling of the second-order average Hamiltonians between the two elements.

Although most of the sequences in Table 2 and Fig. 3 show DQ build-up curves, consistent with the literature (*13, 16, 46*), the sequences that had $\omega_R/\omega_{nut}^S = 2/3$ or larger (Figs. 3D–F) show perturbations within the build-up curves, in the form of small oscillations with a wavelength equal to the length of the sequence. These oscillations are due, in part, to contributions from recoupling between the rf field and the rotor spinning. The oscillations were seen to increase as the chemical shift difference between

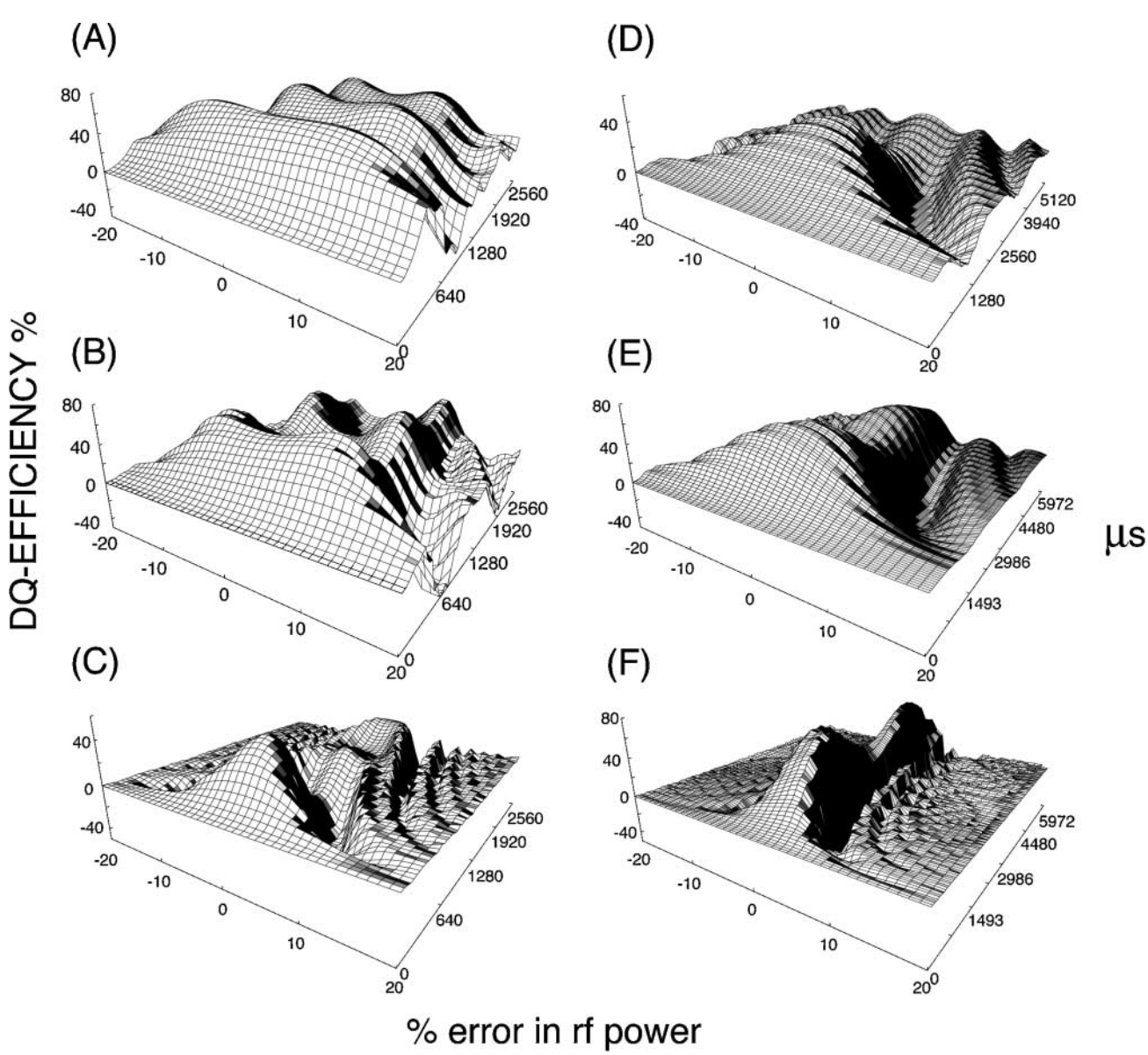

FIG. 3. Simulated DQ recoupling efficiencies as a function of t_{exec} ($t_{rec} = t_{exec}$) and rf power for the [2,3-$^{13}C_2$] succinic acid spin system, with a dipolar coupling of 2150 Hz, CSA taken from Ref. (*51*), typical tensor orientations, using the R element 90_0270_{180} in (A)–(E) and the element $60_0300_{180}60_0$ in (E) and (F). The following DQ recoupling symmetries were used: (A) $R14_2^6$ at $\omega_R = 7143$ Hz; (B) $R14_4^5$ at $\omega_R = 14286$ Hz; (C) $R14_4^{-2}$ at $\omega_R = 14286$ Hz; (D) $R12_{10}^5$ at $\omega_R = 41670$ Hz; (E) $R12_{10}^5$ at $\omega_R = 35715$ Hz; and (F) $R12_{10}^{-1}$ at $\omega_R = 35715$ Hz. The rf error refers to an error in ω_{nut}^S relative to an rf power of 50 kHz. The values used in the simulations were the same as in Table 2.

the two nuclei increased, and as a result, very low DQ quantum efficiencies resulted (less than 10%) in the simulations of the glycine spin system. These sequences were therefore thought to be of little use in broadband recoupling.

Simulations were also carried out for a simple 180° R element, although the results were not given in Table 2, due to the fact that, so far, we have not been able to find any sequences that efficiently recouple the glycine spin system. Most of the sequences do, however, recouple succinic acid, as well as alanine spin systems, giving relatively good DQ efficiencies. It seems that the solution of using p elements instead of longer R elements to obtain broadband DQ recoupling at high spinning rates is rather limited, so we did not investigate the possible use of this R element further. The element has, however, been used successfully in a recent publication where it was used in heteronuclear recoupling (*47*).

The succinic acid spin system was simulated in order to examine the rf-error stability (error in ω_{nut}^S) of the various RN sequences noted earlier. As can be seen from Fig. 3, there is a significant difference in the stability in rf error between different

sequences. While the $R14_2^6$ sequence shows broad DQ recoupling with nearly no dependence on the relative ω_{nut}^S within an allowed error of ±20% (Fig. 3A), a sequence like $R12_{10}^{-1}$ (Fig. 3F) has close to no DQ efficiency when the ω_{nut}^S has an error of only ±2%. Furthermore, it can be seen in Fig. 3 that sequences like $R14_4^5$ (Fig. 3B) are far better than the $R14_4^{-2}$ sequence (Fig. 3C), and the $R12_{10}^5$ sequence (Fig. 3E) far better than the $R12_{10}^{-1}$ sequence (Fig. 3F). The bandwidth over which the sequence effectively recouples the DQ term depends on the length of the DQ recoupling time ($t_{exec} + t_{rec}$, in Fig. 1B). For short DQ recoupling times, all the sequences seems independent of the relative rf error, as can be seen in Fig. 3. The longer the sequence, the larger the effects of accumulated phase errors, as a function of rf tilt angle, and the more dependent the sequences become on the error in ω_{nut}^S. The rf characteristics for several of the sequences at t_{exec} at maximum DQ efficiency are given in Table 2.

When comparing the results of the simulations in Table 2, and the relative phase angle used on consecutive R elements given in the last column of Table 1, a correlation between the stability toward errors in ω_{nut}^S and the angle between the successive R elements ($|2\varphi|$) can be observed. The dependence on the symmetry number n is believed to come from the ability of consecutive pulses to remove rf errors for pulses p out of phase with each other, while the effects will be additive when the pulses are of the same phase. *RN* sequences that have successive R elements with an absolute phase difference ($|2\varphi|$) close to p show good rf stability and can give positive DQ efficiencies with as much as 10–20% error in ω_{nut}^S. However, sequences that have successive R elements with $|2\varphi| < \pi/2$ give efficient DQ recoupling only if the error in ω_{nut}^S is very small (<5%), examples being $R14_4^{-2}$ (Fig. 3C), and $R12_{10}^{-1}$ (Fig. 3F), and these sequences were therefore not investigated further.

After selecting out all those sequences that have poor rf stability and recoupling efficiency, we were left with only a few sequences. We tested their ability to recouple under off-resonance conditions for the three spin systems. [2,3-$^{13}C_2$]alanine and [2,3-$^{13}C_2$]succinic acid gave similar results, although in general, a broader DQ recoupling region was observed for succinic acid than alanine. Figure 4 shows the simulated broadband recoupling of [2,3-$^{13}C_2$]alanine with the sequences $R16_6^5$, $R18_8^5$, and $R18_{10}^5$ as a function of the transmitter offset from the center frequency. Figure 4A shows that there is a plateau at DQ recoupling efficiencies of 61.3% that is nearly independent of the rf off-resonance, in a region ±13 kHz from the center frequency, at a recoupling time equal to 600 ms. The bandwidth in this region is about 26 kHz. The DQ efficiency is somewhat dependent on the offset as well as the recoupling time ($t_{exec} + t_{rec}$), and at longer recoupling times somewhat large dependencies on the relative transmitter frequency were seen. The efficient bandwidth of an R element will depend on the rf field, and might give only small errors at certain frequencies, but when these errors are added, one will see that the region in which the DQ recoupling efficiency is usable will be restricted as the recoupling time is changed. This will, however, not be a problem at fields up to 800 MHz proton frequency, since the sequence will be able to recouple a region of at least 130 ppm at this field strength.

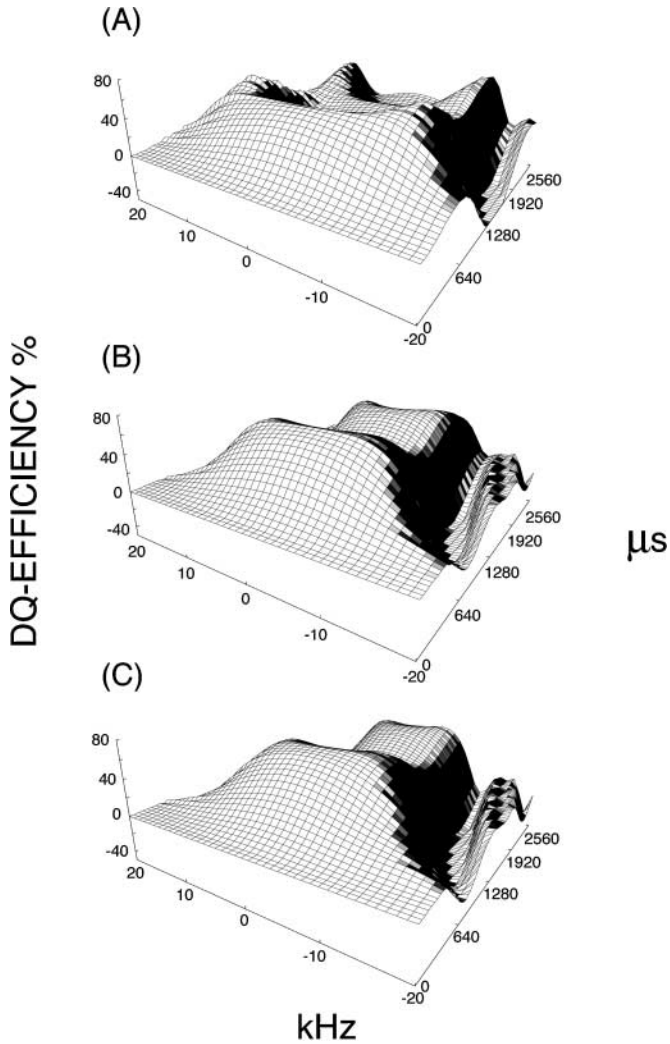

FIG. 4. Simulated DQ recoupling efficiencies as a function of chemical-shift offset from the center frequency between the two spins of [2,3-$^{13}C_2$]alanine and t_{exec} ($t_{rec} = t_{exec}$), using the R element 90_0270_{180}. The system used in the simulations was based on the CSA tensors and orientations given in Ref. (*52*), and the crystal structure given in Ref. (*48*). (A). The DQ recoupling symmetry $R16_6^5$ at $\omega_R = 18750$ Hz, (B) $R18_8^5$ at $\omega_R = 22222$ Hz, (C) $R18_{10}^5$ at $\omega_R = 27778$ Hz. ω_{nut}^S was 50 kHz in all experiments. The offset was calculated from the difference between the transmitter frequency and the center frequency between the two spins.

Figures 4B and 4C show the recoupling of the $R18_8^5$ and $R18_{10}^5$ sequences, respectively. The bandwidth of the recoupling of $R18_8^5$ is slightly larger than for $R18_{10}^5$, and the bandwidth and DQ efficiency were found to be ±11 kHz and 72.6%, and ±10 kHz and 72.2%, respectively, for the two sequences at their maximum DQ efficiency. The DQ efficiency curves are similar for the two sequences, except for the slightly smaller bandwidth of the $R18_{10}^5$ sequence.

In Fig. 5, the simulated DQ recoupling efficiency as a function of off-resonance frequency is shown for [1,2-$^{13}C_2$]glycine. For this spin system, the effects of the relative resonance frequency are much larger than for alanine and succinic acid, and this probably has to do with the limited bandwidth of the pulse sequence, and to contributions from CSA. The DQ efficiency falls to 30–50%. It needs to be added that our simulations search for solutions at high spinning rates, and relatively high magnetic fields (14.1 T). The isotropic peaks of glycine will be separated by approximately 20 kHz at this magnetic field strength, and the $\omega_{nut}^{S} = 50$ kHz will not result in exact π rotations even if the transmitter is placed in the center between the two peaks. The effects of the second-order anisotropy terms will also be greater for glycine at this magnetic field than at lower fields, for which the majority of the other sequences were developed. Furthermore, the limited bandwidth of the recoupling element affects resonances from nuclei with large CSAs, and in simulations, where the nutation frequency is large enough to ensure π rotations for all the sidebands, the effects of CSA could be observed in systems with small dipolar couplings. These effects become particularly important in simulations on spin systems with large CSAs and relatively small dipolar couplings, where drastic reductions in the DQ efficiency were observed. For instance, when the dipolar couplings were reduced to only 200 Hz (~3.4 Å) for a spin system with CSA tensors and orientations equal to that of [1,2^{13}C]glycine, the DQ efficiency fell to only 17% of its theoretical maximum for $R14_2^6$. Minor increases in DQ efficiencies were observed as a function of relatively drastic increases in the nutation frequency, indicating that insufficient CSA suppression can drastically reduce the dipolar couplings. However, the $R14_2^6$ sequence shows excellent broadband performance in the simulations on the spin system of glycine at 14.1 T (Fig. 5A), even though the CSA is not fully removed by spinning. This probably has to do with the fact that the $R14_2^6$ sequence have very few second-order cross terms between the CSA and the dipolar coupling, and other results of insufficient CSA suppression are of little effect for large dipolar couplings. In simulations of the C7 sequence with this spin system, large effects of CSA were observed.

From Fig. 5 one can easily see that the $R18_8^5$ (Fig. 5C) and $R18_{10}^5$ (Fig. 5D) sequences, which have more or less the same bandwidth properties with glycine, both show far better off-resonance stability than the $R16_6^5$ sequence (Fig. 5B). This is exactly the opposite of what was observed in the simulation of alanine (Fig. 4). The DQ efficiency is, however, less for $R18_{10}^5$ than the two other sequences. The relative bandwidth of the sequences at their maximum DQ recoupling efficiency was shown to be approximately ±7 kHz, ±5 kHz, ±7 kHz, and ±6 kHz in Figs. 5A–D. Furthermore in all of the planes, oscillations like the ones observed in Figs. 3D–E can be observed. These oscillations are seen only at large off-resonance frequencies in the case of $R14_2^6$ (Fig. 5A), and increase for the other sequences (Fig. 5) under off-resonance conditions. They are thought to be due to errors introduced by the limited

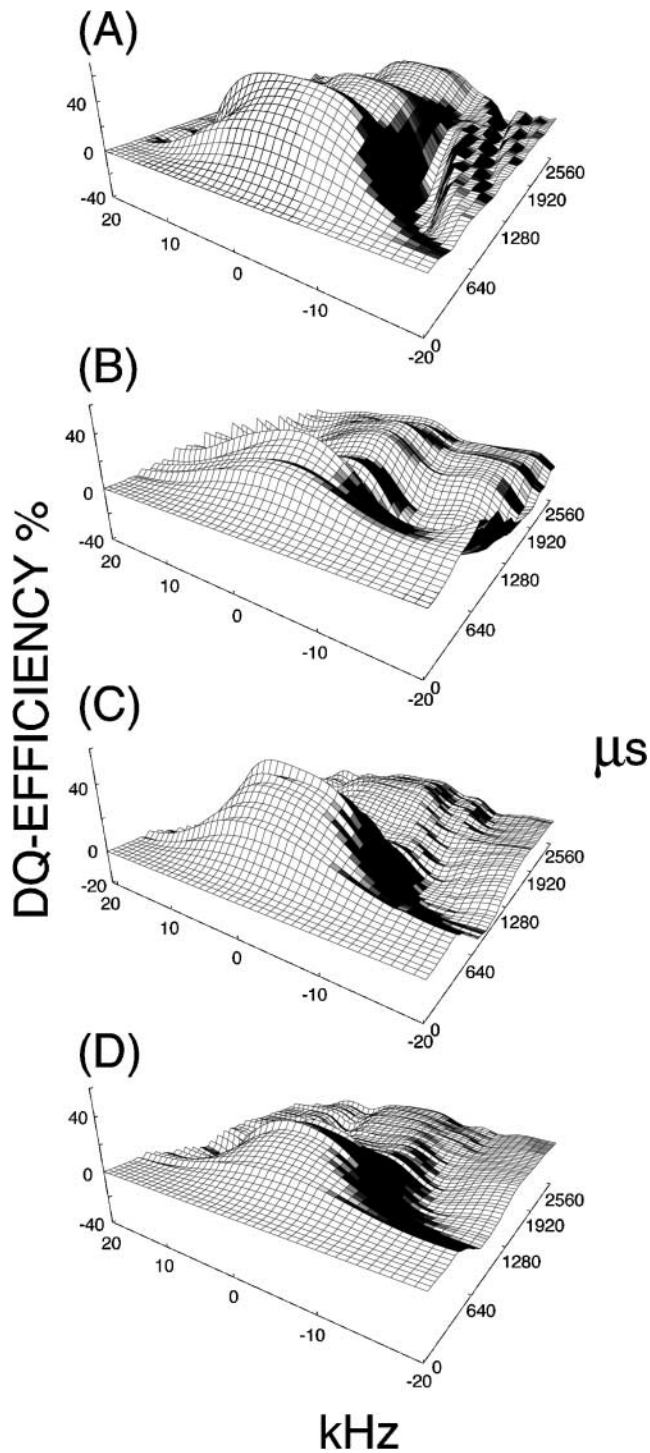

FIG. 5. Simulated DQ recoupling efficiencies as a function of chemical-shift offset from the center frequency between the two spins of [1,2-$^{13}C_2$]glycine and $t_{exec}(t_{rec} = t_{exec})$, using the R element 90_0270_{180}. The system used in the simulations was based on the CSA tensors and orientations given in Ref. (*53*), and the crystal structure given in Ref. (*54*). (A). The DQ recoupling symmetry $R14_2^6$ at $\omega_R = 7143$ Hz; (B) $R16_6^5$ at $\omega_R = 18750$ Hz; (C) $R18_8^5$ at $\omega_R = 22222$ Hz, and (D) $R18_{10}^5$ at $\omega_R = 27778$ Hz. ω_{nut}^{S} was 50 kHz in all experiments. The offset was calculated from the difference between the transmitter frequency and the center frequency between the two spins.

bandwidth of the pulses, introducing errors that are chemical-shift dependent.

From these simulations, the following sequences seem promising for use in practical NMR experiments with $5 > \omega_R/\omega^S_{nut} > 1.8$: $R18^7_4$, $R14^5_4$, $R20^7_6$, $R16^5_6$, $R18^5_8$, and $R18^5_{10}$. All these sequences gave the shortest DQ excitation time in simulations with the R element 90_0270_{180}, and except for the $R18^5_{10}$ sequence, they all have $\kappa_{lm\lambda\mu} < 0.130$ and were seen to reach the maximum DQ efficiency in simulations within ≈750 ms, for succinic acid.

Experimental Results

Maximum DQ efficiency as a function of the recoupling time has been measured experimentally for the sequences, $R16^5_6$, $R18^5_8$, and $R18^5_{10}$, and the experimental data are given in Fig. 6. As can be seen from Fig. 6, the experimental data decay with time and never show DQ efficiencies close to the theoretical maximum of 73% (*13*). Several relaxation parameters are thought to contribute to the decay in DQ efficiency, one being the relaxation due to residual heteronuclear dipolar couplings to protons. The contribution from residual heteronuclear proton couplings cannot, however, be simulated, since there is no good model for the proton spin bath. To be able to obtain a good fit between the simulated and the experimental data, we used the following empirical equation,

$$I_{Obs}(t) = \sum_m I_{Sim}(t) * a_m \exp\left(-\left(t/T_{2,a_m}\right)^n\right), \qquad [11]$$

where $t = t_{exec} + t_{rec}$, a_m is a normalized constant (fraction) such that $\sum_m a_m = 1$, and T_{2,a_m} is the decay constant of the fraction a_m. Equation [11] was applied to take account of the relaxation occurring during the DQ recoupling.

The simple double-exponential ($n = 1, m = 2$ Eq. [11]) model suggested by Carravetta *et al.* (*46*) gave a considerably better fit to the data than a single exponential, although a slightly better fit was obtained by fitting to two Gaussians ($n = 2$, Eq. [11]), or increasing the number of functions. The Gaussian function was used in Fig. 6.

A close look at the fit of the DQ build-up curves to the experimental data show that there is a discrepancy that increases with increasing recoupling times. This increase in error between the fit and the experimental data was also seen in the original C7 sequence paper (*13*) as well as in the $R14^6_2$ papers (*16, 46*). Several reasons are possible for this error, both of experimental origin and in the fitting of the experimental data. The *RN* sequences will, to some extent, be influenced by delays in the phase transmitter, giving an efficient phase and pulse length somewhat different from the ones given by the *RN* selection rules, and the pulse program. Caravatti *et al.* (*46*) showed recently that these errors could be partly removed by adjusting the phase angles. This fix does not completely remove the effects at long recoupling times, and with limited phase resolution. Unstable rotor frequency, ±20 Hz at 14250 kHz, is also thought to contribute to the discrepancy, although this contribution is thought to be limited, since the relative errors appear to be larger for $R18^5_8$ and $R18^5_{10}$ sequences, than for $R16^5_6$ sequences, which had the least stable rotor speed. The fitting error might also be due to the limited ability of the simple addition of decay functions to fully take care of relaxation. In addition to this the natural abundance ^{13}C background might influence the shape of the curve, especially at long DQ build-up times, in ways that are not taken into consideration in the simulation of the DQ excitation curves.

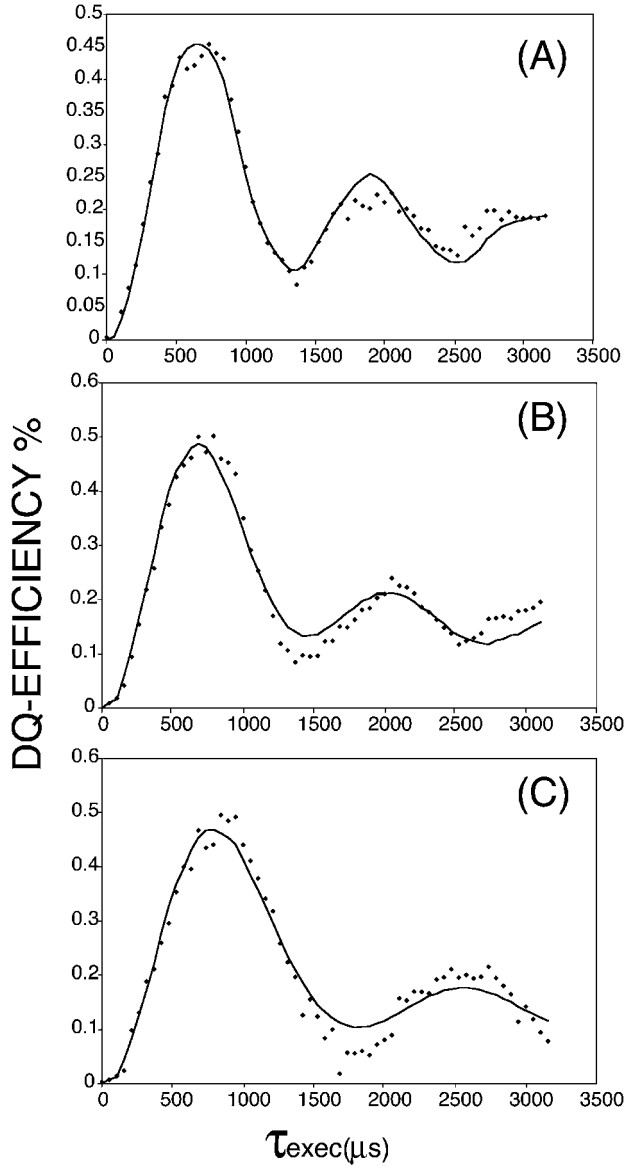

FIG. 6. The experimental data on DQ recoupling of [2,3-$^{13}C_2$]alanine, incrementing $t_{exec}(t_{rec} = t_{exec})$, using the R element 90_0270_{180}, together with the best experimental fits from simulations (see text for further details). (A) $R16^5_6$ at $\omega_R = 14250 \pm 20$ Hz; (B) $R18^5_8$ at $\omega_R = 16889 \pm 10$ Hz; and (C) $R18^5_{10}$ at $\omega_R = 21111 \pm 5$ Hz. The ω^S_{nut} was 38 kHz and centered between the two nuclei. The line represents the best fit, and the points represent experimental data.

As can be seen in Fig. 6, all the three sequences, $R16_6^5$, $R18_8^5$, and $R18_{10}^5$, give satisfying least-squares fit between experimental and simulated data. In Fig. 5A the dipolar coupling was found to be −1990 Hz, Fig. 5B gave a dipolar coupling of −2080 Hz, and in Fig. 5C the dipolar coupling was found to be −2000 Hz. The absolute error in the recoupled dipolar couplings was estimated to be approximately 100 Hz in all the fitted curves. These dipolar couplings correspond to 1.563, 1.540, and 1.560 Å, respectively, which is only between 1.1 and 2.5% longer than the distance measured by neutron diffraction (*48*). The agreement between our measured distances and the neutron diffraction measurements shows that all three sequences can be used for distance measurements in labeled compounds. Furthermore, the recoupling efficiency was found to be between 40 and 50% DQ yield in all three cases, which we consider to be good for these kind of sequences.

INADEQUATE Using RN Sequences and Phase Cycling

The DQ recoupling sequences given above can all be used in INADEQUATE types of experiments, using sequences like the one shown in Fig. 1B. The phase cycling of the pulse sequence, and the incrementing of the recoupling sequence, must be timed to give correct phase and shift values. We have shown earlier an example of the use of *RN* sequence in INADEQUATE spectroscopy (*42*), but then only refer to the phase cycling suggested by Brinkmann *et al.* (*37*) in the case of *CN* sequences, and the phase cycling for the *RN* sequences is easier than for *CN* sequences. The phase cycling needs to: (i) select signals that go through DQ coherences in the t_1 interval; and (ii) be constructed so that a pure phase spectrum can be obtained. We used the TPPI procedure to obtain a pure phase signal (*49*). Since the *RN* sequence does not depend on the incrementation of the phases of the recoupling sequence, if every q (the number of $R + R'$ elements, see Fig. 1A) is kept even, the sequence will only need to be incremented due to the phase development as a function of the incremented delay. The TPPI phase cycling gives us the following phase incrementation for the excitation part of INADEQUATE sequence (Eq. [12]),

$$\Phi_{Prep} = \frac{\pi}{4} m_1, \qquad [12]$$

where m_1 is 0, 1, 2, 3, . . . and incremented for every increment in t_1. The DQ filtering is obtained by standard incrementation of the read pulse (Φ_{Read} in Fig. 1B) and acquisition (Φ_{Rec} in Fig. 1B) for DQ filtering,

$$\Phi_{Read} = \frac{\pi}{2} + \frac{\pi}{2} m_2 \qquad [13]$$

$$\Phi_{Rec} = -\frac{\pi}{2} m_2, \qquad [14]$$

where m_2 is incremented from 0, 1, 2, 3 to obtain DQ filtering of the signal. The recoupling sequence Φ_{Rec} does, however, need to be incremented by $1/2\,\omega_r t_1$ in order to take care of the evolution of the rotor phase during the incremented delay t_1. This gives us then Φ_{Rec}:

$$\Phi_{Rec} = \frac{\pi}{2} + \frac{1}{2}\omega_r t_1 + \frac{\pi}{2} m_2. \qquad [15]$$

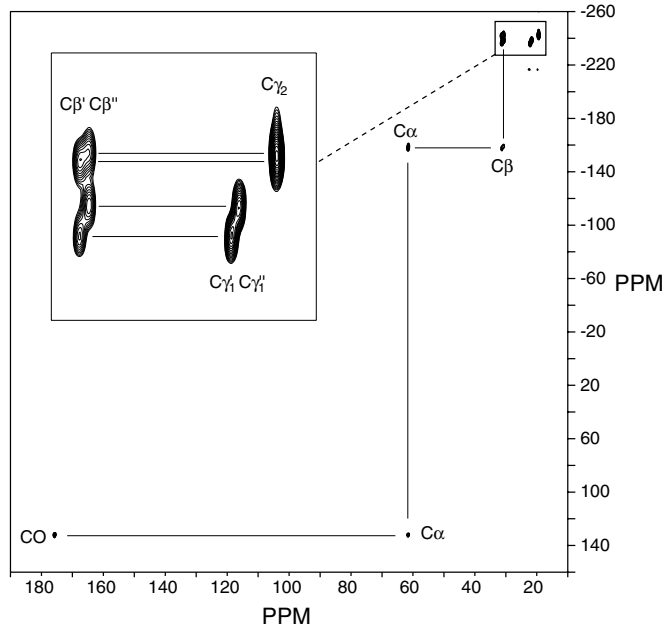

FIG. 7. 2D INADEQUATE spectrum of [U-^{13}C,^{15}N]valine obtained with the sequence in Fig. 1(B) using the $R18_{10}^5$ symmetry sequence and the R element 90_0270_{180}. The expanded C_β and C_γ region of the 2D spectrum is shown in the insert. The spinning rate ω_R was 30 kHz, ω_{nut}^S was 54 kHz, and $t_{rec} = t_{exec} = 778\ \mu$s was applied. 2D spectra were Fourier-transformed with NMR-Pipe (*56*) and displayed with PIPP (*57*). The vertical DQ axis was referenced arbitrarily to the transmitter frequency at 0 ppm.

The phase-sensitive two-dimensional spectrum (Fig. 7) was obtained by a complex Fourier transform in the t_2 dimension and a cosine Fourier transform of the t_1 dimension.

The application of the $R18_{10}^5$ sequence within INADEQUATE at a spinning rate of 30 kHz is shown in Fig. 7 for [U-^{13}C, ^{15}N]valine. The rf frequency was offset 3 kHz upfield from the center frequency between the C═O and Cα of valine, showing that the $R18_{10}^5$ sequence is capable of recoupling spins with relative large differences in ICS and CSA under off-resonance conditions, just as was shown for this sequence in the simulation (Fig. 5D). To obtain good signal-to-noise, the decoupling rf power was increased to 96 kHz during the acquisition, in order to avoid recoupling with the spinning frequency (*50*), and this doubled the DQ signal as compared to that obtained at 76 kHz.

The two $C_{\gamma 1}$ and $C_{\gamma 2}$ are well separated in Fig. 7, although closer inspection of the C_β and C_γ region of the spectrum, shown as an insert in Fig. 7, indicates that it is possible to distinguish two

different C_β and two $C_{\gamma 1}$ resonances. The chemical shifts can be correlated as shown in Fig. 7, and it can be seen that the two downfield resonances of C''_β and $C''_{\gamma 1}$ belong to the same molecule as C''_β and $C''_{\gamma 1}$. The different chemical shifts are assumed to be due to the two different molecular structures observed in the unit cell of valine (*60*). The slight difference in chemical shift of the two C_β and $C_{\gamma 1}$ carbons of valine was also observed by Ye *et al.* (*61*). The ability to resolve the two distinct unit cell structures of valine demonstrates the excellent resolution obtained in INADEQUATE spectroscopy.

The $R18^5_{10}$ sequence is suited for recoupling at even higher spinning rates, and when the ω^S_{nut} is increased to 70 kHz, a ω_R as high as 39 kHz can be used. At these spinning rates, indirect detection can be used in solid-state NMR (*40, 41*), The sequence might therefore be useful for recoupling of carbon nuclei in indirectly detected solid-state NMR.

4. CONCLUDING REMARKS

The different possible *RN* sequences found by using the selection rules introduced by Carravatti *et al.* have been investigated, and a large series of new DQ recoupling sequences have been suggested. We believe that the sequences, $R18^7_4$, $R14^5_4$, $R20^7_6$, $R16^5_6$, $R18^5_8$, and $R18^5_{10}$, listed in order of increasing ω_R/ω^S_{nut}, will be of greatest value in multidimensional solid-state NMR investigations of proteins. Which one of these sequences to apply will depend on the problem that is being investigated. The new sequences will be particularly useful in situations where high magnetic fields and large CSAs, as well as large dipolar couplings, make high MAS rates necessary. The sequences are thought to be useful for low gamma nuclei recoupling, for instance, as a part of sequences using high MAS rates and proton detection. No efficient DQ recoupling technique has until now been usable for these kind of sequences. We believe that some of these DQ recoupling techniques will also find use in selective recoupling of dipolar couplings in the future. The sequences can, for instance, be used at low power, where their bandwidth will be limited, and only recouple spins with chemical shifts within a narrow region of the spectrum.

5. EXPERIMENTAL

Samples

[2,3 $^{13}C_2$]Alanine sample was purchased from Cambridge Isotopes Inc. and diluted to 10% w/w with unlabeled alanine before recrystallization. [U-^{13}C, ^{15}N]Valine was used as obtained from Cambridge Isotopes Inc.

NMR Experiments

All spectra were obtained on a Bruker DRX 600 NMR spectrometer with a 14.1 T Magnex wide-bore magnet, and a 2.5-mm Bruker HXY triple resonance probe, at room temperature, with no measures to avoid frictional heating from the sample rotation.

A composite pulse of four 90_0–270_{180} elements and a standard adamantane sample was used to measure the powers on the S channel. The relative phase used in the individual *R* element was optimized by running series of experiments that had 0.1° differences in phase. The phase that gave the maximum DQ efficiency over a large time interval (particularly in the area between first and second maximum) was chosen. Phase resolutions of <0.1° were not achievable with the current instrument. Generally a phase of −0.2° from the one given by the selection rules was found to work the best.

The rf power on the I channel during DQ recoupling was kept constant at 126.6 kHz in all experiments. The rf-decoupling power was set to 76.6 kHz during the acquisition in experiments performed at spinning rates below 25 kHz, and 96.6 kHz at spinning rates of 30 kHz. TPPM decoupling (*55*) was applied during the acquisition, and 1024 data points were acquired. The intensities obtained in the experiments where from peak integrals, relative to peak integrals in ordinary CP experiments normalized to 1.

A total of 192 data points were collected in the t_1 dimension, while 768 data points were obtained in the t_2 dimension. 2D spectra were Fourier-transformed using NMRPipe (*56*) and displayed by the use of PIPP (*57*). Linear prediction was applied in both dimensions. 1D spectra were obtained by Fourier transformation with the Bruker XWINNMR software. The chemical-shift scale was obtained by referencing to adamantane (38.4 ppm).

Simulations

To evaluate the ability of the different pulse sequences to distinguish between different rotations of the carbonyl group the simulation program SIMPSON was used (*58*). A powder average of 100 crystallite sets of α and β angles calculated by REPULSION (*59*) and 10γ angles were used in the simulation. The DIRECT method (*58*) was used for simulations of the *RN* sequences. All simulations were carried out at a proton frequency of 600 MHz. All simulations converged with ca. 1000 crystallites, although larger numbers of crystallites (ca. 4000) were used to confirm the convergence when unusual behavior of the DQ curves was observed. Least-squares fitting was used to evaluate the quality of the fit, and for optimizing the dipolar couplings.

ACKNOWLEDGMENTS

This research was supported by NIH Grant R01 GM43215, and by a Norwegian Science Foundation postdoctoral fellowship NFR134918/432 (to P.E.K.). The WSU NMR Center equipment was supported by NIH Grants RR0631401 and RR12948, NSF grants CHE-9115282 and DBI-9604689, and a grant from the Murdock Charitable Trust. We are grateful to Andreas Brinkmann for explaining the phase cycling principle of SPC14, and John Young for helping with the Fourier transformation of the 2D spectrum. The SIMPSON simulation package was generously donated by N. C. Nielsen at the University of Aarhus. Data processing and viewing software were generously donated by Frank Delaglio and Dan Garrett at NIH.

REFERENCES

1. M. H. Levitt, D. P. Raleigh, F. Creuzet, and R. G. Griffin, Theory of homonuclear spin pair systems in rotating solids, *J. Chem. Phys.* **92,** 6347–6364 (1990).
2. R. G. S. Spencer, K. J. Halverson, M. Auger, A. E. McDermott, A. G. Griffin, and P. T. Lansbury, Application of solid state NMR to the determination of protein structure, *Biochemistry* **30,** 10382 (1991).
3. R. Tycko and G. Dabbagh, Measurements of nuclear magnetic dipole-dipole couplings in magic angle spinning NMR, *Chem. Phys. Lett.* **173,** 461–465 (1990).
4. J. H. Ok, R. G. S. Spencer, A. E. Bennett, and R. G. Griffin, Homonuclear correlation spectroscopy in rotating solids, *Chem. Phys. Lett.* **197,** 389–395 (1992).
5. A. E. Bennett, J. K. Ok, R. G. Griffin, and S. Vega, Chemical-shift correlation spectroscopy in rotating solids-radio frequency-driven dipolar recoupling and longitudinal exchange *J. Chem. Phys.* **96,** 8624–8627 (1992).
6. J. M. Griffiths, K. V. Lakshmi, A. E. Bennett, J. Raap, C. M. van der Wielen, J. Lugtenburg, J. Herzfeld, and R. G. Griffin, Dipolar correlation NMR-spectroscopy of a membrane-protein, *J. Am. Chem. Soc.* **116,** 10178–10181 (1994).
7. T. Fujiwara, A. Ramamoorthy, K. Nagayama, K. Hioka, and T. Fujito, Dipolar HOHAHA under MAS conditions for Solid-State NMR, *Chem. Phys. Lett.* **212,** 81–84 (1993).
8. W. Zhu, C. A. Klug, and J. Schaefer, Measurement of dipolar coupling within isolated spin-1/2 homonuclear pairs by CEDRA NMR, *J. Magn. Reson. A* **108,** 121–123 (1994).
9. B.-Q. Sun, C. M. Rienstra, P. R. Costa, J. R. Williamson, and R. G. Griffin, 3D N-15-C-13-C-13 chemical shift correlation spectroscopy in rotating solids, *J. Am. Chem. Soc.* **119,** 8540–8546 (1997).
10. B.-Q. Sun, P. R. Costa, D. Kosciko, P. T. Lansbury, Jr., and R. G. Griffin, Internuclear distance measurements in solid-state nuclear-magnetic-resonance-dipolar recoupling via rotor synchronized spin locking, *J. Chem. Phys.* **102,** 702–707 (1995).
11. D. M. Gregory, D. M. Mitchell, J. A. Stringer, S. Kilhne, J. C. Shields, J. Callahan, M. A. Metha, and G. P. Drobny, Windowless dipolar recoupling—The detection of weak dipolar couplings between spin-1/2 nuclei with large chemical-shift anisotropies, *Chem. Phys. Lett.* **246,** 654–663 (1995).
12. N. C. Nielsen, H. J. Jakobsen, H. Bildsoe, and M. H. Levitt, Double-quantum homonuclear rotary resonance—Efficient dipolar recovery in magic-angle-spinning nuclear-magnetic-resonance, *J. Chem. Phys.* **101,** 1805–1812 (1994).
13. Y. K. Lee, N. D. Kurur, M. Helmle, O. Johannessen, N. C. Nielsen, and M. H. Levitt, Efficient dipolar recoupling in the NMR of rotating solids—A sevenfold symmetrical radiofrequency pulse sequence, *Chem. Phys. Lett.* **242,** 304–309 (1995).
14. M. Hohwy, H. J. Jacobsen, M. Eden, M. H. Levitt, and N. C. Nielsen, Broadband dipolar recoupling in the nuclear magnetic resonance of rotating solids: A compensated C7 pulse sequence, *J. Chem. Phys.* **108,** 2686–2694 (1998).
15. C. M. Rienstra, M. E. Hatcher, L. J. Mueller, B. Q. Sun, S. W. Fesik, and R. G. Griffin, Efficient multispin homonuclear double-quantum recoupling for magic-angle spinning NMR: C-13-C-13 correlation spectroscopy of U-C-13-erythromycin A, *J. Am. Chem. Soc.* **120,** 10602–10612 (1998).
16. M. Carravetta, M. Eden, X. Zhao, A. Brinkmann, and M. H. Levitt, Symmetry principles for the design of radiofrequency pulse sequences in the nuclear magnetic resonance of rotating solids, *Chem. Phys. Lett.* **321,** 205–215 (2000).
17. X. Feng, Y. K. Lee, D. Sandstrom, M. Eden, H. Maisel, A. Sebald, and M. H. Levitt, Direct determination of a molecular torsional angle by solid-state NMR, *Chem. Phys. Lett.* **257,** 314–320 (1996).
18. Y. Ishii, T. Terao, and M. Kainosho, Relayed anisotropy correlation NMR: Determination of dihedral angles in solids, *Chem. Phys. Lett.* **256,** 133–140 (1996).
19. M. Hong, J. D. Gross, and R. G. Griffin, Site-resolved determination of peptide torsion angle phi from the relative orientations of backbone N–H and C–H bonds by solid-state NMR, *J. Phys. Chem. B* **101,** 5869–5974 (1997).
20. K. Schmidt-Rohr, Torsion angle determination in solid 13C-labeled amino acids and peptides by separated-local-field double-quantum NMR, *J. Am. Chem. Soc.* **118,** 7601–7603 (1996).
21. Y. Li, R. J. Appleyard, W. A. Shuttleworth, and J. N. S. Evans, Time resolved solid-state REDOR NMR measurements on EPSP synthase, *J. Am. Chem. Soc.* **116,** 10799–10800 (1994).
22. Y. Li, F. Krekel, C. A. Ramilo, N. Amrhein, and J. N. S. Evans, Time-resolved solid-state REDOR NMR studies of UDP N-acetylglucosamine enolpyruvyl transferase, *FEBS Lett.* **377,** 208–212 (1995).
23. A. M. Christensen and J. Schaefer, Solid-state NMR determination of intra-inermolecular 31P-13C distances for shikimate 3-phosphate and [1-13C]glyphosate bound to enolpyruvylshikimate-3-phosphate synthase, *Biochemistry* **32,** 2868–2893 (1993).
24. L. M. McDowell, A. Schmidt, E. R. Cohen, D. R. Studelska, and J. Schaefer, Structural constraints on the ternary complex of 5-enolpyrovylshikimate-3-phosphate synthase from rotational-echo double-resonance NMR, *J. Mol. Biol.* **256,** 160–171 (1996).
25. S. J. Opella, NMR and membrane proteins, *Nature Struct. Biol.* **4,** 845–848 (1997).
26. T. A. Cross and S. J. Opella, Solid-state NMR structural studies of peptides and proteins in membranes, *Curr. Opin. Struct. Biol.* **4,** 574–581 (1994).
27. P. T. Lansbury, P. R. Costa, J. M. Griffiths, E. J. Simon, M. Auger, K. J. Halverson, K. D. A., Z. S. Hendsch, T. T. Aschburn, R. G. S. Spencer, B. Tidor, and R. G. Griffin, Structural model for the beta-amyloid fibril based on interstrand alignment of an antiparallel beta-sheet comprising a C-terminal peptide, *Nature Struct. Biol.* **2,** 990–998 (1995).
28. T. L. S. Benzinger, D. M. Gregory, T. S. Burkoth, H. Miller-Auer, D. G. Lynn, R. E. Botto, and S. C. Meredith, Propagating structure of Alzheimer's beta-amyloid((10-35)) is parallel beta-sheet with residues in exact register, *Proc. Natl. Acad. Sci. USA* **95,** 13407–13412 (1998).
29. R. Tycko, Prospects for resonance assignments in multidimensional solid-state NMR spectra of uniformly labeled proteins, *J. Biomol. NMR* **8,** 239–251 (1996).
30. J. Pauli, B. van Rossum, H. Förster, H. J. M. de Groot, and H. Oschkinat, Sample optimization and identification of signal patterns of amino acid side chains in 2D RFDR spectra of the alpha-spectrin SH3 domain, *J. Magn. Reson.* **143,** 411–416 (2000).
31. A. E. McDermott, T. Polenova, A. Bockmann, K. W. Zilm, E. K. Paulsen, R. W. Martin, and G. T. Montelione, Partial NMR assignments for uniformly (C-13, N-15)-enriched BPTI in the solid state, *J. Biomol. NMR.* **16,** 209–219 (2000).
32. M. T. Zell, B. E. Padden, D. J. W. Grant, M.-C. Chapeau, I. Prakash, and E. J. Munson, Two-dimensional high-speed CP/MAS NMR spectroscopy of polymorphs. 1. Uniformly C-13-labeled aspartame, *J. Am. Chem. Soc.* **121,** 1372–1378 (1999).
33. S. K. Straus, T. Bremi, and R. R. Ernst, Resolution enhancement by homonuclear J. decoupling in solid-state MAS NMR, *Chem. Phys. Lett.* **262,** 709–715 (1996).
34. S. Dusold and A. Sebald, Dipolar recoupling under magic-angle spinning conditions, *Ann. Rep. NMR Spectrosc.* **41,** 185–264 (1999).

35. M. Hohwy, C. M. Rienstra, C. P. Jaroniec, and R. G. Griffin, Fivefold symmetric homonuclear dipolar recoupling in rotating solids: Application to double quantum spectroscopy, *J. Chem. Phys.* **110,** 7983–7992 (1999).

36. A. E. Bennett, C. M. Rienstra, J. M. Griffiths, W. Zhen, P. T. Lansbury, Jr., and R. G. Griffin, Homonuclear radio frequency-driven recoupling in rotating solids, *J. Chem. Phys.* **108,** 9463–9479 (1998).

37. A. Brinkmann, M. Edén, and M. H. Levitt, Synchronous helical pulse sequences in magic-angle spinning nuclear magnetic resonance: Double quantum recoupling of multiple-spin systems, *J. Chem. Phys.* **112,** 8539 (2000).

38. Y. Ishii, C-13-C-13 dipolar recoupling under very fast magic angle spinning in solid-state nuclear magnetic resonance: Applications to distance measurements, spectral assignments, and high-throughput secondary-structure determination, *J. Chem. Phys.* **114,** 8473–8483 (2001).

39. M. Hong, Solid-state dipolar INADEQUATE NMR spectroscopy with a large double-quantum spectral width, *J. Magn. Reson.* **136,** 86–91 (1999).

40. Y. Ishii and R. Tycko, Sensitivity enhancement in solid-state 15N NMR by indirect detection with high-speed angle spinning, *J. Magn. Reson.* **142,** 199–204 (2000).

41. I. Schnell, B. Langer, S. H. M. Soentjens, M. H. P. van Genderen, R. P. Sijbesma, and H. W. Spiess, Inverse detecion and heteronuclear editing in 1H-15N correlation and 1H-1H double-quantum NMR spectroscopy in the solid state under fast MAS, *J. Magn. Reson.* **150,** 57–70 (2001).

42. P. E. Kristiansen and J. N. S. Evans, Band-selective pulses in solid-state INADEQUATE NMR, submitted for publication.

43. A. Brinkmann and M. Levitt, Symmetry principles in the nuclear magnetic resonance of spinning solids: Heteronuclear recoupling by generalized Harmann-Hahn sequences, *J. Chem. Phys.* **115,** 357–384 (2001).

44. U. Haeberlen, "High Resolution NMR in Solids, Advances in Magnetic Resonance," Academic Press, New York (1976).

45. A. Brinkmann, M. Edén, X. Feng, H. Luthman, L. Eriksson, A. Graslund, O. N. Antzutkin, and M. H. Levitt, 39th Experimental NMR Conference, Asilomar, 1998.

46. M. Carravetta, M. Edén, O. G. Johannessen, H. Luthman, P. J. E. Verdegem, J. Lugtenburg, A. Sebald, and M. H. Levitt, Estimation of carbon-carbon bond lengths and medium-range internuclear distances by solid-state nuclear magnetic resonance, *J. Am. Chem. Soc.* **123,** 10628–10638 (2001).

47. X. Zhao, J. L. Sudmeier, W. W. Bachovchin, and M. H. Levitt, Measurement of NH bond lengths by fast magic-angle spinning solid-state NMR spectroscopy: A new method for the quantification of hydrogen bonds, *J. Am. Chem. Soc.* **123,** 11097–11098 (2001).

48. M. S. Lehman, T. F. Koetzle, and W. C. Hamilton, Precision neutron diffraction structure determination of protein and nucleic acid components. I. The crystal and molecular structure of the amino acid L-alanine, *J. Am. Chem. Soc.* **95,** 2657–2660 (1972).

49. A. G. Redfield and S. D. Kuntz, Quadrature FT NMR: Multiplex for dual detection, *J. Magn. Reson.* **19,** 250 (1976).

50. M. Ernst and B. H. Meier, Heteronuclear spin decoupling under high frequency magic-angle sample spinning, talk presented at the 2nd Alpine Conference on Solid-State NMR, 2001.

51. N. R. Jagannathan, Carbon-13 chemical shielding tensors in alkanedicarboxylic acids. Influence of molecular geometry on the carboxyl carbon tensors in alkanedicarboxylic acids and related compounds, *Magn. Reson. Chem.* **27,** 941–946 (1989).

52. A. Naito, S. Ganapathy, K. Akasaka, and A. McDowell, Chemical shielding tensor and 13C-14N dipolar splitting in single crystals of l-alanine, *J. Chem. Phys.* **74,** 3190–3197 (1981).

53. R. A. Haberkorn, R. E. Stark, H. van Willigen, and R. G. Griffin, Determination of bond distances and bond angles by solid-state nuclear magnetic resonance. 13C and 14N NMR study of glycine, *J. Am. Chem. Soc.* **103,** 2534–2439 (1981).

54. P. G. Jönsson and Å. Kvick, Precision neutron diffraction structure determination of protein and nucleic acid components. III. The crystal and molecular structure of the amino acid a-glycine, *Acta. Crystallogr. B* **28,** 1827–1833 (1972).

55. A. E. Bennett, C. M. Rienstra, M. Auger, K. V. Lakshmi, and R. G. Griffin, Heteronuclear decoupling in rotating solids, *J. Chem. Phys.* **103,** 6951–6958 (1995).

56. F. Delaglio, S. Grzesiek, G. W. Vuister, G. Zhu, J. Pfeifer, and A. Bax, NMRpipe—A multidimensional spectral processing system based on UNIX pipes, *J. Biomol. NMR* **6,** 277–293 (1995).

57. D. S. Garrett, R. Powers, A. M. Gronenborn, and G. M. Clore, A common-sense approach to peak picking in 2-dimensional, 3-dimensional, and 4-dimensional spectra using automatic computer-analysis of contour diagrams, *J. Magn. Reson. B* **95,** 214–220 (1991).

58. M. Bak, J. T. Rasmussen, and N. C. Nielsen, SIMPSON: A general simulation program for solid-state NMR spectroscopy, *J. Magn. Reson.* **147,** 296–330 (2000).

59. M. Bak and N. C. Nielsen, Relative orientation of chemical shielding and dipolar coupling tensors: Mixed single- and double-quantum homonuclear rotary resonance nuclear magnetic resonance of rotating solids, *J. Chem. Phys.* **106,** 7587–7599 (1997).

60. K. Torrii and Y. Iitaka, The crystal structure of L-valine, *Acta. crystallogr. B* **26,** 1317–1326 (1970).

61. C. Ye, R. Fu, J. Hu, L. Hou, and S. Ding, Carbon-13 chemical shift anisotropies of solid amino acids, *Magn. Reson. Chem.* **31,** 699–704 (1993).